APPLIED AND ENVIRONMENTAL MICROBIOLOGY, Feb. 1997, p. 724–733 Vol. 63, No. 2
0099-2240/97/$04.00+0

Computer-Assisted Laser Scanning and Video Microscopy for Analysis of *Cryptosporidium parvum* Oocysts in Soil, Sediment, and Feces

LYNNE J. ANGUISH AND WILLIAM C. GHIORSE*

Section of Microbiology, Division of Biological Sciences, Cornell University, Ithaca, New York 14853

Received 1 May 1996/Accepted 7 August 1996

A computer-assisted laser scanning microscope equipped for confocal laser scanning and color video microscopy was used to examine *Cryptosporidium parvum* oocysts in two agricultural soils, a barnyard sediment, and calf fecal samples. An agar smear technique was developed for enumerating oocysts in soil and barnyard sediment samples. Enhanced counting efficiency and sensitivity (detection limit, 5.2×10^2 oocysts · g [dry weight]$^{-1}$) were achieved by using a semiautomatic counting procedure and confocal laser scanning microscopy to enumerate immunostained oocysts and fragments of oocysts in the barnyard sediment. An agarose-acridine orange mounting procedure was developed for high-resolution confocal optical sectioning of oocysts in soil. Stereo images of serial optical sections revealed the three-dimensional spatial relationships between immunostained oocysts and the acridine orange-stained soil matrix material. In these hydrated, pyrophosphate-dispersed soil preparations, oocysts were not found to be attached to soil particles. A fluorogenic dye permeability assay for oocyst viability (A. T. Campbell, L. J. Robertson, and H. V. Smith, Appl. Environ. Microbiol. 58:3488–3493, 1992) was modified by adding an immunostaining step after application of the fluorogenic dyes propidium iodide and 4′,6-diamidino-2-phenylindole. Comparison of conventional color epifluorescence and differential interference contrast images on one video monitor with comparable black-and-white laser-scanned confocal images on a second monitor allowed for efficient location and interpretation of fluorescently stained oocysts in the soil matrix. This multi-imaging procedure facilitated the interpretation of the viability assay results by overcoming the uncertainties caused by matrix interference and background fluorescence.

The increasing availability of laser scanning microscopy (LSM) and video microscopy for applications in environmental microbiology and microbial ecology (4, 5, 7, 14, 18, 19, 31), especially for biofilm analysis (6, 24, 25, 27, 28, 32, 47, 48), has fostered the development of new and improved methods for microscopic analysis of environmental samples. These methods can be expected to have positive impacts on research problems in environmental microbiology by providing better techniques for single-cell identification and enumeration, as well as for assessment of in situ cellular activity and viability. Furthermore, the development of improved methods in environmental microbiology can help to alleviate urgent environmental problems, such as the identification, enumeration, and assessment of viability of pathogenic agents that pose a public health risk, such as the oocysts of the waterborne parasite *Cryptosporidium parvum* (23).

The involvement of *C. parvum* oocysts in waterborne outbreaks of gastrointestinal disease has been well documented. Outbreaks in drinking water have occurred in the United States in Texas, New Mexico, and Georgia (13, 22, 33, 40) and most recently in Wisconsin (29). However, the actual sources of contamination (i.e., the identity of infective oocysts) have not always been determined. Furthermore, the mechanisms of oocyst survival and transport in the environment are unknown. Overland transport of oocysts in feces and manure from domestic farm animals and infected wildlife into water courses has been suggested as a possible source of oocysts in rural watershed areas (30, 34, 40, 41). However, difficulties with detection sensitivity and assessment of viability when oocyst numbers are small, as well as the inability of current methods to distinguish between species and strains of *Cryptosporidium*, hinder firm conclusions on this point. In addition, issues of environmental transport and fate are obfuscated by a lack of information on in situ microscale environmental factors and fundamental biological properties of oocysts that affect their transport and survival in watershed environments.

Questions of identification and enumeration have been addressed to some extent for water samples by using immunofluorescence (IF) staining and conventional microscopic techniques (1, 20, 42, 43) or flow cytometry (45, 46), and some environmentally oriented viability studies have been done by using infectivity (16, 17), excystation (38), and fluorescent dye exclusion (permeability) (8, 36, 37) assays to assess oocyst viability. Except for the infectivity assay (16, 17), this work depended on conventional epifluorescence microscopy for the final analysis. While conventional microscopic techniques have proved to be adequate for analysis of oocysts in low-turbidity water samples, they have not been satisfactory for analysis of oocysts in highly turbid water (46). Alternative methods such as fluorescence in situ hybridization with rRNA probes are promising (23, 46), but in the end, detection of oocysts by conventional epifluorescence microscopy of concentrated particulate material will still be problematic due to the increased opacity and textural complexity of the sample matrix.

LSM with confocal epifluorescence imaging and optical sectioning of semiopaque samples allow for the virtual elimination of interference from background autofluorescence and out-of-focus haze in the image plane (7, 19). This provides a promise

* Corresponding author. Mailing address: Section of Microbiology, Division of Biological Sciences, Wing Hall, Cornell University, Ithaca, NY 14853. Phone: (607) 255-3086. Fax: (607) 255-3904. E-mail: wcg1@cornell.edu.

of improved methods of visualizing oocysts in particulate samples, limited only by the depth of penetration of the laser beam. These computerized instruments also provide a number of useful automated features, such as automatic stage position control and the ability to store, process, and analyze high-resolution optical sections (4, 12, 26, 27). The latter is essential for stereo viewing to show three-dimensional spatial relationships. Combining LSM with color video microscopy allows for simultaneous imaging of real-time fluorescence color with laser-scanned images. This combination is particularly useful for multiple fluorescence and molecular probe applications where color discrimination is important.

Our long-term goal is to develop more sensitive methods for detection, identification, enumeration, and testing the viability of *C. parvum* oocysts for routine use with environmental samples. To achieve this, we must first apply the most advanced microscopic equipment to improve the sensitivities of the available assays. Subsequent work will be directed at transferring this technology for use in more routine procedures that can be done with more conventional equipment.

In this article we describe the development of computer-assisted LSM and color video microscopy techniques that improved our ability to identify and enumerate, and to determine microscale interactions and assess viability of, *C. parvum* oocysts in the semiopaque matrices of soils, sediments, and fecal samples.

MATERIALS AND METHODS

Soil, barnyard sediment, and fecal samples. Collamer silt loam (fine-silty, mixed, mesic Aquic Hapludalfs) (approximately 300 g) was collected from the top 25 cm of an agricultural field at Cornell University, Ithaca, N.Y., in a sterile screw-top 500-ml container and stored at 4°C until used. This soil consisted of 7% sand, 74% silt, and 19% clay. In some experiments, when a higher concentration of silt and clay was desired, we used the silt-clay fraction from another silt loam soil collected in Trumansburg, N.Y. (47% sand, 47% silt, and 6% clay). This was air dried and stored at room temperature (RT) before being sieved to recover the silt-clay fraction. Organic barnyard sediment samples (uncharacterized) were collected from a calf hutch drainage area at the Cornell University Teaching and Research Center in Harford, N.Y., where cryptosporidiosis is endemic in young calves. The hutches were placed on crushed rock approximately 15 cm deep (stone size, 3 to 5 cm). At depths below 8 cm, an organic sediment consisting of an approximately 1:1 ratio of silt and settled calf manure with decomposed straw bedding had accumulated under the influences of rainfall and animal and human movement around the hutches. The top 8 cm of stones was removed, and the sediment in the deeper layer was collected with a sterile spatula into clean 240-ml plastic snap cap sample cups (catalog no. 78-500-4000-008; Krackler Scientific, Albany, N.Y.). The samples were immediately placed on ice in a cooler for transport to the laboratory and stored at 4°C for processing within 24 h. Fecal samples were collected from 6- to 20-day-old Holstein calves housed in the hutches by palpating the rectum to induce defecation into the sample cups. Samples from each calf were transported and stored as described above. Immediately upon arrival, smears were made of each fecal sample on microscope slides, which were allowed to air dry overnight. The smears were then stained with a monoclonal fluorescent-antibody kit specific for *Cryptosporidium* oocysts (Hydrofluor Combo [Meridian Diagnostics, Cincinnati, Ohio, or EnSys Environmental Products, Inc., Research Triangle Park, N.C.]) according to the manufacturer's recommended protocol. Stained samples were examined for the presence of oocysts under differential interference contrast (DIC) and epifluorescence optics with blue excitation for the conjugated fluorescein isothiocyanate (FITC) label with a 100× (numerical aperture [NA], 1.3) Neofluar DIC objective lens. Fecal samples showing a high number ($>10^6$ per g of feces) of apple-green fluorescent, 4- to 6-μm, spherical (i.e., *Cryptosporidium*) oocysts with internal structure in DIC imaging were pooled. The fecal pool was strained through a fine-mesh tea strainer to remove large particulates and then stored at 4°C in a screw-capped glass bottle for 3 to 4 months before being used to seed soils for enumeration studies.

Agar smear technique for oocyst enumeration in soil and sediment. The moisture content of soils and barnyard sediments was determined by drying duplicate subsamples (approximately 10 g each) overnight at 105°C. The weight of the subsamples was recorded before and after drying. The water content was calculated as a percentage of dry weight. The remaining sample was treated as follows. Triplicate 2.5-g subsamples were dispersed at a 1:10 (wt/vol) dilution in 0.1% sodium pyrophosphate (NaPP) (pH 7.2) and mixed on a rotary shaker at 150 rpm for 30 min at RT as previously described (21). Dispersed samples were allowed to settle for 1 min to allow large particulates to settle out. Ten milliliters of the supernatant (not including large floating organic matter such as wood chips) was collected by pipette. Smears were prepared for enumeration by adding formaldehyde to a final concentration of 0.5% to fix the dispersed supernatant suspension, and then molten agar was added to a final concentration of 0.1%. Duplicate 10-μl samples were smeared over an area of 1 cm^2 as previously described (21). Dried smears were flooded with 0.01 M phosphate-buffered saline (PBS) (pH 7.2) containing 0.05% Tween 20 for 5 min and then stained by using an IF staining procedure that consisted of covering the smear alternately with 25 μl of 1× Hydrofluor primary and secondary antibody reagents and washing, essentially as described in the manufacturer's protocol. Stained smears were gently blotted and mounted with 10 μl of 0.3 M 1,4-diazabicyclo[2.2.2] octane in 0.1 M PBS under a coverslip sealed with a thin layer of Vaspar (paraffin-petroleum jelly, 1:1). Smears were examined within 8 h with the 100× DIC objective lens (described above) or with a 63× (NA, 1.4) oil immersion phase-contrast objective lens. Oocysts and fragments of oocysts were identified and measured by using simultaneous comparison of conventional epifluorescence images captured by the charge-coupled device (CCD) camera with those produced by the LSM (see instrument details below).

Details of the counting procedure for bacteria in soil and sediment were described previously (3, 21). Counting rules have been established based on the frequency of detection, with a lower frequency demanding that more replicate subsamples and greater numbers of microscopic fields be counted for statistical accuracy. As a compromise with time and operator fatigue, two smears from three replicate subsamples were counted. Samples with fewer than 10 oocysts per 50 fields required that at least 50 fields be counted per smear to achieve less than 40% error. Results are reported as the number of oocysts or oocyst fragments per gram (dry weight [dw]) of soil. When 50 fields were counted per smear (total, 300 fields) with the 63× objective lens, the detection limit was approximately 7.9×10^3 oocysts · g (dw) of $soil^{-1}$.

Semiautomatic counting procedure. In order to improve the sensitivity of this counting procedure (i.e., lower the detection limit), a larger number of fields was examined. This was facilitated by using the LSM version 2.10 software to create a raster pattern of *x* and *y* positions (or fields). Each set of *x* and *y* positions was given a number from 0 to 169 by using the version 2.10 mark-and-find program. Once the glass slide carrying the specimen was in place on the motorized stage, a programmed raster of fields could be examined in series, and any position in the raster pattern could be recalled by keyboard command. With this program, all positions on a smear could be identified by a number up to 169. The entire smear could then be examined in serial sets of 169 fields each. This allowed for a thorough semiautomatic examination of each smear at the high magnification and resolution required for identification without examining the same field twice. The set of commands for this procedure were written and stored as a macro on the LSM host computer hard drive for recall when needed.

Seeding of soil and sediment samples. In order to optimize procedures for confocal imaging of oocysts in soils, the Collamer silt loam was seeded with a suspension of oocysts purified from calf feces by sucrose floatation at a final concentration of approximately 10^6 oocysts · g (dw) of $soil^{-1}$. During purification, the oocysts were not exposed to ethyl acetate or other reagents known to alter their surface properties (15). Oocysts were kindly supplied in a distilled water suspension preserved with an antibiotic mixture by Dwight Bowman, New York State College of Veterinary Medicine, Cornell University, Ithaca, N.Y. The oocyst-soil mixture was dispersed and settled in NaPP as described above. In other experiments, the dispersed and settled soil suspension was seeded after dispersion as follows. One milliliter of dispersed soil suspension was placed in a 1.5-ml microcentrifuge tube. The sample was microcentrifuged (model 59A Fisher Scientific microcentrifuge) for 30 s at maximum speed ($11{,}150 \times g$). The supernatant was replaced with 1 ml of PBS containing approximately 10^6 oocysts, and the suspension was mixed gently with a vortex mixer. Fixative and agar were then added as described above. The Trumansburg silt-clay which had been air dried during storage was rehydrated overnight at 4°C by adding 0.5 ml of Milli-Q (17 to 18 $M\Omega\ cm^{-1}$) water to 2 g of soil. The rehydrated samples were seeded after dispersal and settling with either the purified oocysts or the fecal suspensions as described above.

Agarose-AO mounting procedure for confocal optical sectioning of soil samples. Initially, soil samples were prepared by drying up to 25 μl of dispersed and fixed agar-containing sample on a 1-cm^2 circle on a microscope slide and then staining with the IF procedure as described above. However, this procedure produced drying artifacts and flattened zones at the interfaces of both the coverslip and the slide which were noticeable in stereo images of confocal optical sections. In addition, we were concerned that the added thickness of the smear may have prevented the antibodies from penetrating the entire sample when the usual staining protocol was employed. To overcome these problems, the seeded dispersed soil samples were stained in suspension by using the IF staining protocol (see below), except that the soil was first washed with 1 ml of 0.1 M PBS containing 0.05% Tween 20 to decrease nonspecific binding of the antibodies to soil components. Then, with a truncated micropipette tip, 10 μl of the stained suspension was dropped into the center of a 14-mm-diameter well of a Teflon-coated slide (catalog no. 10-12; Cel-Line Associates, Newfield, N.J.). The specimen drop in the well was immediately mixed with a 10-μl drop of a molten agarose mixture containing 3 parts 1.0% agarose and 1 part 0.1% acridine orange (AO), both in distilled water. The mixing was achieved by quickly coalescing the specimen drop with an agarose-AO drop carried on an 18-mm-square coverslip.

This method produced an agarose-AO-embedded suspension of particulate material which after cooling and solidification of the agarose was approximately 30 μm thick. FITC-stained oocysts, AO-stained soil organic material, and bacteria in the soil particles were imaged at all depths in the agarose-AO suspension with the 488-nm laser excitation and the BP 515-565 emission filter for confocal imaging and optical sectioning. The use of 18-mm-square coverslips was important to minimize the effects of deformation of the coverslip glass in the *z* direction when an oil immersion lens was used.

Dye permeability assay combined with IF staining. The dye permeability assay was essentially the same as that previously described (9) with the addition of IF staining after the dye exposure step. The assay procedure was applied to unfixed seeded soil or sediment, dispersed as described above and settled, or purified oocyst or fecal samples. For each sample, four 100-μl replicate subsamples were removed into 1.5-ml microcentrifuge tubes. Stock solutions of 4′,6-diamidino-2-phenylindole (DAPI) (2 mg/ml in high-pressure liquid chromatography-grade methanol) and propidium iodide (PI) (1 mg/ml in 0.1 M PBS, pH 7.2) were prepared and stored at 4°C in the dark. To each 100-μl subsample, 10 μl of PI and 10 μl of DAPI stock solution were added, and the mixture was vortexed. The mixture was then placed in a 37°C incubator for 1.5 h. After incubation, the mixture was stained by the IF staining procedure in suspension. In this procedure, 10 μl of undiluted Hydrofluor primary antibody was added to each subsample, and the tubes were returned to the incubator for 0.5 h. After the second incubation, 1.0 ml of the PBS solution was added to each tube, the suspensions were vortexed and microcentrifuged, and the supernatant was discarded. The pellets were resuspended into 100 μl of PBS, and 10 μl of undiluted Hydrofluor secondary antibody reagent was added to each tube. The tubes were then incubated for 0.5 h at RT in the dark. After incubation, the tubes were again microcentrifuged, and the pelleted material was washed twice as described above with PBS. The final pellets were resuspended in 100 μl of 1,4-diazabicyclo[2.2.2] octane PBS and stored at 4°C until analyzed (within 72 h). We noted that unfixed oocysts in soil or sediment samples were susceptible to damage during mixing. Other workers have also noted that oocysts can be damaged by sand (11, 35). Thus, the damage could have been caused by abrasion during mixing the sand in the sample. To avoid such damage, the samples were mixed very gently either by resuspending the pellets with truncated micropipette tips or by very slow vortexing. This precaution ensured that the oocyst wall was not damaged by abrasion with soil mineral particles. Purified oocysts and fecal preparations could be vortexed at high speeds without noticeable damage to the oocyst wall or patchy immunostaining.

For microscopic analysis, a 10-μl portion of each stained subsample was placed on an air-dried agar-coated slide and mounted under a 22-mm-square coverslip. Mounted slides were put aside for 30 s before examination to allow water in the sample to diffuse into the dried agar layer, creating a hydrated agar matrix around the sample. The agar-coated slides were prepared by air drying an even film of molten 1% purified agar produced by spreading 1 ml of a 1% agar solution in distilled water on an alcohol-cleaned glass slide. Samples were observed with the 100× (NA, 1.3) oil immersion Neofluar DIC objective lens with both epifluorescence and DIC imaging. For optimum imaging, the 1.4-NA condenser lens top element was also immersed in oil. The UV and the triple excitation filter combinations were used for conventional epifluorescence, and the 488-nm laser line combined with the BP 515-565 (green) or the LP 590 (red) emission filter was used for laser-excited epifluorescence. Conventional DIC imaging was achieved with the usual polarizer-Wallaston prism-polarizer combinations. The first polarizer filter was removed for laser-scanned DIC because the laser light was already polarized and the filter significantly reduced the laser-induced fluorescence signal, thus degrading confocal images.

Microscopy. All samples were examined with a Zeiss LSM-210 laser scanning microscope equipped for conventional video microscopy as well as LSM. This instrument has four light sources (an external argon laser emitting at 488 and 514 nm, an internal helium-neon laser emitting at 633 nm, a 12-W halogen lamp, and a 50-W mercury arc lamp) and two imaging detectors (a photomultiplier for reflected light and epifluorescence and a silicone diode for transmitted light). This allowed for laser-scanned and conventional transmission and epifluorescense imaging of the same microscopic field. In the laser scanning mode, a focused laser beam is scanned through the objective lens in a raster pattern across a defined area of the specimen by galvanometer scanning mirrors driven by a digitally controlled scan generator. During laser scanning, the argon laser was operated at the lowest current possible (3.99 A with laser light output of 7.9 W) in order to reduce photobleaching of fluorescent specimens. The laser could be operated at either a constant current or a constant light output. The latter gave the best results when laser scanning was used for optical sectioning. Photobleaching was also retarded by placing an interference filter in the laser beam path to lower the laser intensity to 10% of its output. Our instrument is equipped with 63× and 100× oil immersion objectives (NA, 1.3 or 1.4) and an oil immersion condenser lens (NA, 1.4) which can be used for phase-contrast, DIC, bright-field, and epifluorescence imaging in both conventional and laser scan modes. Laser-scanned confocal imaging was done in the reflected-light (epifluorescence) mode. All laser-scanned images were viewed on an RGB video monitor (Sony Trinitron model CPD-1402E character display). For laser-scanned epifluorescence, including confocal epifluorescence, band pass filters are placed in the light path before the photomultiplier detector in order to select for specific fluorescence wavelengths. We used a BP 515-565 filter to select for green and an LP 590 filter to select for red fluorescence imaging. Confocal epifluorescence imaging is done by inserting a 30-μm pinhole in front of the photomultiplier at the proper confocal distance. Conventional images can be viewed through 10× eyepieces or through an attached color CCD video camera (Optronics model VI-470). CCD video images were displayed on a second color video monitor (Sony Trinitron model PVM 1343MD). For the epifluorescence applications described in this paper, three filter combinations were used with the conventional mercury arc source: (i) blue excitation (BP 450-490, FT 510, and LP 520 filters [Carl Zeiss, Inc.]), (ii) UV excitation (BP 360/40, FT 395, and LP 397 filters [Chroma, Brattleboro, Vt.]), and (iii) triple-band excitation (excitations at 402.5/13, 495.5/17, and 571/26 and emissions at 426/23, 531/32, and 627/53 [Chroma]).

The laser scanning and conventional optical systems of the LSM 210 were controlled through the host computer and control panel software (LSM version 2.10; Carl Zeiss, Inc.). Control panel commands allowed for selection of imaging mode, laser wavelength, laser scan rate, 20× to 160× electronic zoom factors, laser attenuator filters, and control of *x*, *y*, and *z* movement of the stage and contrast and brightness settings for the laser-scanned images on the monitor. The software also contained programs for *z* sectioning for optical sectioning and stereo imaging. Other composite image reconstruction and simultaneous viewing options are also available in the LSM 210 software. Other useful software options included image storage, processing and enhancement such as frame and line averaging, and size and area measurements of captured images, as well as full *x*, *y*, and *z* position control of the motorized stage. The latter allowed for position storage and creation of raster patterns for automated scanning of specimens.

Digital images and imaging parameters produced in the laser scan modes were stored temporarily on a 2-megabyte (MB) frame grabber or permanently on a 32-MB disk drive in the host computer. For long-term storage, the digital images were transferred via an IEEE linkage to a 20-MB mass storage cartridge (Bernoulli BoxII; Iomega) through an image analysis computer (Kontron; ELEKTRONK GmbH) with VIDAS 2.1 image processing and LSM-NET software (Carl Zeiss, Inc.). Laser-scanned images could also be recorded on a Sony UP-850 black-and-white videographic thermal printer, a Sony UP-3000 color printer, or a 35-mm photographic film through a color image video recorder (Matrix Multicolor; Matrix Instruments, Inc.). Conventional microscopy images were recorded through the LSM 210 camera port fitted with a Nikon dual channel optivar unit engineered to reflect 100% light to either channel. One channel was connected to a Zeiss MC-100 35-mm camera system for conventional photomicrography; the other was connected to the CCD video camera. CCD images were recorded either on the Sony color or the Sony black-and-white printer or in the Matrix camera system. Kodak HC (or ELITE) or EK 160T (color) slide film was used for recording primary images on film. Color prints were made directly from color slides by using the fluorochrome process.

RESULTS AND DISCUSSION

Enumeration of oocysts in soil and sediment. Recent work in our laboratory has focused on improving analytical microscopy methods for examining microorganisms in semiopaque samples (18, 19). Part of this work has addressed the critical problem of microscopic detection limits on the sensitivity of counting bacteria and determining bacterial viability in oligotrophic sediments (18, 21). We have examined the parameters which limit the sensitivity of microscopic assays and have demonstrated (18) that greater sensitivity can be achieved by using conventional counting procedures provided that a greater number of microscopic fields can be examined.

As part of this work, we have developed an AO-agar smear technique for counting bacteria in soil (44) and adapted it for bacteria in shallow aquifer sediments (3). Recently, we improved this method for counting bacteria in very dry, oligotrophic subsurface sediments (21). This basic agar smear technique has proved to be useful for microscopic analyses of microorganisms in a wide variety of sample types, especially those containing low numbers of microorganisms in a particulate matrix (21).

We adapted this method for enumeration of oocysts in soils and barnyard sediments by first determining that seeded oocysts could be stained by the commonly used Hydrofluor IF staining kit. After staining, we showed that we could enumerate oocysts with less than 30% error and 60 to 95% recovery efficiency when they were seeded at elevated concentrations ($>10^5 \cdot g\ [dw]^{-1}$) in agricultural soil. In one experiment, two soil samples were seeded with approximately 5.3×10^5 and

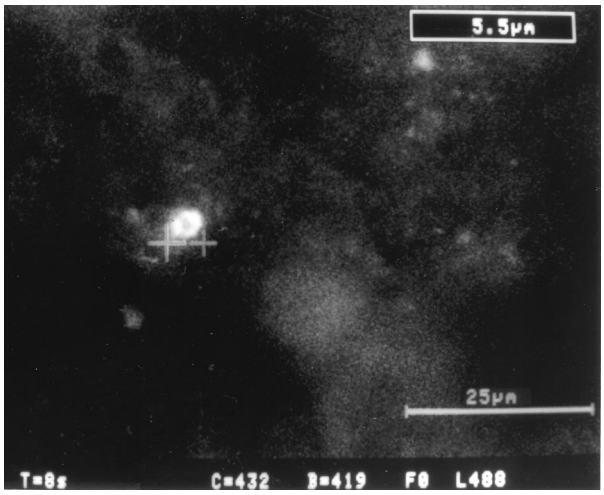

FIG. 1. Laser-scanned epifluorescence image of a typical immunostained oocyst counted in the barnyard sediment sample (see criteria for identification in the footnotes to Table 1). This apple-green fluorescent object was first identified by conventional epifluorescence and DIC imaging (not illustrated). It was then analyzed further by confocal laser scanning epifluorescence with 488-nm excitation. To record this image, the 63× (NA, 1.4) oil immersion DIC objective lens was used with an electronic zoom factor of 40× (final magnification, ×2,520) and an 8-s-per-frame scanning time. An overlay produced by the LSM 210 measurement software gives the oocyst diameter in the box at the upper right.

5.3×10^6 oocysts · g $(dw)^{-1}$, respectively. The actual counts were $(5.0 \pm 1.0) \times 10^5$ and $(3.2 \pm 0.8) \times 10^6$ · g $(dw)^{-1}$, respectively. The estimated efficiencies of recovery were 94 and 60%, respectively.

We then sought to test the method on barnyard sediments naturally contaminated with oocysts. Samples were obtained in late October from an ephemeral channel approximately 2 m downgrade (10 to 15% slope) from a calf hutch area which housed approximately 30 young Holstein calves ranging in age from 1 to 56 days. One calf housed 2 m upgrade from the sample location was confirmed to be shedding oocysts on the day of collection. There had been a heavy rain on the day before collection. Sediment samples were prepared by the agar smear technique, stained with the usual IF procedure, and examined for oocysts and oocyst fragments. Immunostained oocysts showing no internal features (Fig. 1) and oocyst fragments identified by their IF were measured, further analyzed by confocal LSM, and counted by the semiautomated counting procedure to increase the number of fields counted (Table 1). The sample illustrated in Table 1 contained $(1.3 \pm 0.7) \times 10^4$ oocysts · g $(dw)^{-1}$ with no internal features (Fig. 1) and $(2.7 \pm 0.7) \times 10^5$ particles that appeared to be oocyst wall fragments · g $(dw)^{-1}$. No intact oocysts or oocysts with any internal sporozoite structures were observed in the sample. Therefore, we concluded that the number of potentially infective oocysts in the sample was less than the detection limit of the analysis (5.2×10^2 · g $[dw]^{-1}$). However, several oocysts with no internal features (Fig. 1) were observed (Table 1). Further analysis by optical sectioning (not illustrated, but see Fig. 2C for an example) showed this object to be a flattened oocyst envelope. It is interesting that most of the IF-stained objects encountered in this sample were objects of the correct shape and size to be fragments of oocyst walls. Given the history of endemic cryptosporidiosis in this calf-housing area, these structures were most likely degraded *C. parvum* oocyst walls. However, because the Hydrofluor kit antibodies have been shown to cross-react with a number of species of freshwater algae (39), it is also possible that algae or other soil microorganisms could account for some of the fluorescent oocyst-like structures.

An important point to be gathered from Table 1 is that the detection limit of counting (in this case, 5.2×10^2 g $[dw]^{-1}$) was achieved by counting a large number (4,573) of microscope fields. Obtaining the data in Table 1 required approximately 5.45 h of counting, which was facilitated by the use of the LSM 210 search-and-find software and a user-designed macro for an automated stage position control. Use of this semiautomatic counting method allowed the greater number of fields to be counted with high accuracy, which provided a substantial improvement in sensitivity over manual counting procedures. Use of this method also minimized operator fatigue, which usually limits the number of fields that can be counted. We estimated that the use of the automated procedure improved the practical detection limit (with the 63× objective) by a factor of

TABLE 1. Counting data for a single barnyard sediment sample for indigenous *Cryptosporidium* oocysts obtained with the agar smear technique and the semiautomated counting procedure

Subsample	Smear	No. of fields counted[a]	Approx time (h)	No. of IF-stained[b] objects · g $(dw)^{-1}$		
				Oocyst wall fragments[c]	Oocysts with no internal features[d]	Oocysts with internal features[e]
I	1	672	0.80	73	1	0
	2	672	0.80	33	3	0
II	1	762	0.90	40	3	0
	2	787	0.95	115	9	0
III	1	840	1.00	83	1	0
	2	840	1.00	140	6	0
Total		4,573	5.45	$(2.7 \pm 0.7) \times 10^5$	$(1.3 \pm 0.7) \times 10^4$	$<5.2 \times 10^2$

[a] Each field was 0.1164 mm^2; the 63× (NA, 1.4) oil immersion DIC lens and 10× eyepiece were used.

[b] See Fig. 1 and Materials and Methods. Totals are means ± standard deviations, calculated by multiplying the mean number of objects per field by a conversion factor of 2.6×10^6 fields · g $(dw)^{-1}$. The moisture content of the sample was ca. 25%.

[c] Structure with correct size (<6-μm diameter), shape (semicircular or oval), and IF-FITC fluorescence (apple-green under 450- to 490-nm excitation) to be derived from a *C. parvum* oocyst, with no internal sporozoite structure in DIC imaging.

[d] Structure with the correct size (4- to 6-μm diameter), shape (circular or slightly oval), and IF-FITC fluorescence (apple-green under 450- to 490-nm excitation filter) to be a *C. parvum* oocyst but with no internal sporozoite structures in DIC imaging (see, e.g., Fig. 1).

[e] Same as footnote *d* except that internal sporozoite structures are seen in DIC imaging (see, e.g., Fig. 2B).

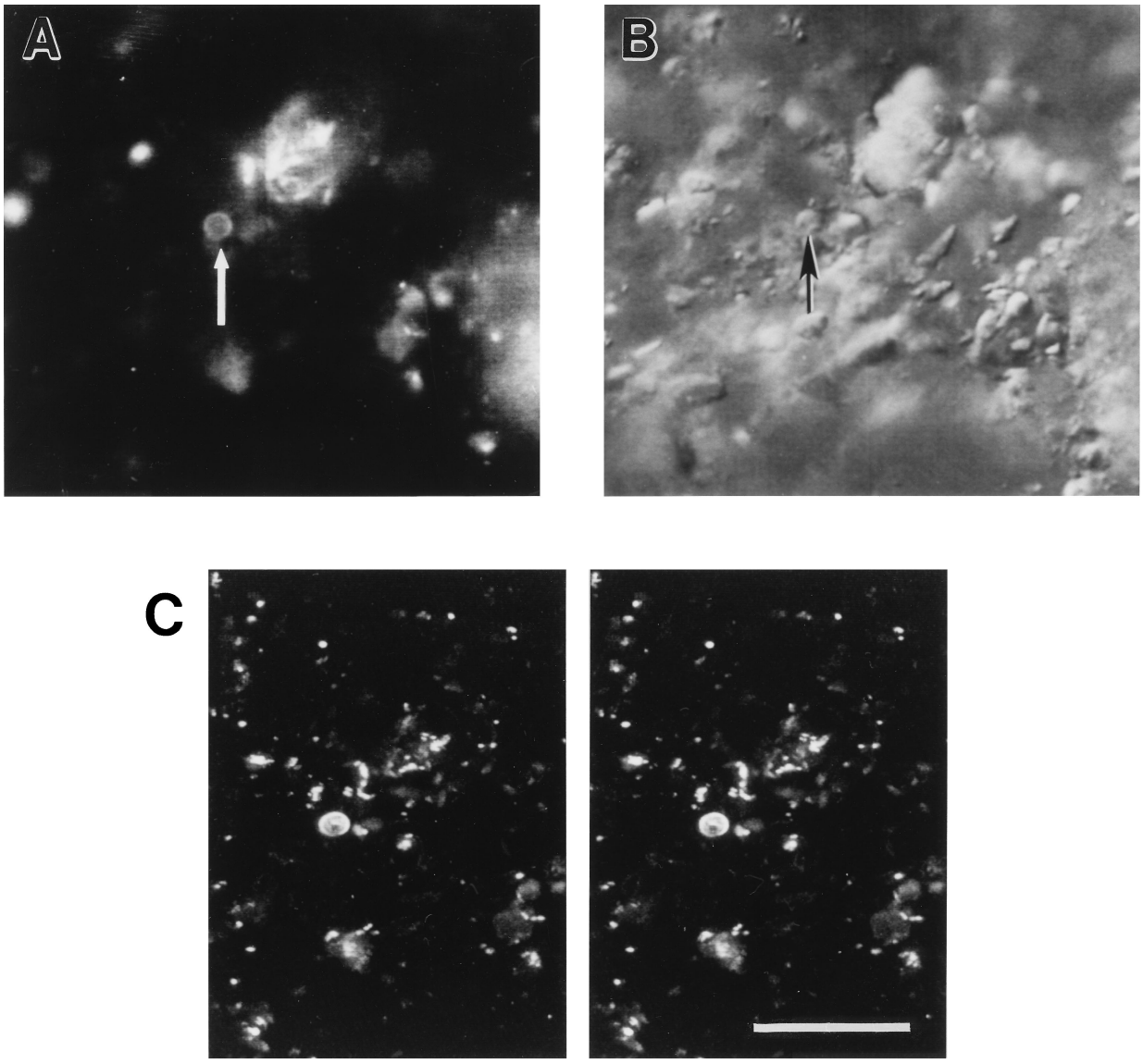

FIG. 2. Comparison of conventional epifluorescence (A) and DIC (B) images with a stereo image (C) composed of 15 overlaid confocal laser-scanned optical sections, displayed here as a right-left stereo pair. All images show the same *C. parvum* oocyst (arrows) seeded in Collamer silt loam soil. The oocyst-containing soil suspension was first stained by the IF procedure and then mounted and counterstained with the AO-agarose procedure as described in Materials and Methods. The stereo pair images (C) were produced by the LSM 210 software from a series of 15 stored confocal optical sections recorded at 2.0-μm depth intervals (total depth, 30 μm). Each optical section was recorded by using 488-nm laser excitation, an 8-s-per-frame scanning time with 16-line averaging, and an electronic zoom factor of 30× (final magnification, ×1,890). The images in panels A and B were recorded with the color CCD camera, printed with the color printer, and then reproduced in black and white at the same magnification as for panel C for comparison. The 63× (NA, 1.4) oil immersion DIC lens was used for all images. Bar, 25 μm.

approximately 15 simply by increasing the number of fields that could be counted in a reasonable amount of time. Further application of this method showed that the same detection limit as achievable in an experimental system in which oocysts were seeded at or near the detection limit (46a).

The ability to examine a larger number of microscopic fields with minimum operator fatigue is only one approach to improving the sensitivity of this assay. Another approach would be to increase the field area by using a lower-power objective lens. This approach is restricted by the resolution limit of the lens and brightness of the fluorescent signal, both of which limit the ability to identify fluorescent objects in the soil matrix. A third approach would be to release oocysts from the soil matrix and concentrate them; then, an optimum imaging and counting procedure such as that described here could be applied to count the concentrated oocysts. New procedures based on these strategies currently are being developed in our laboratory for counting of oocysts in soil and sediment and turbid water (46a).

Confocal optical sectioning and stereo imaging of oocysts in soil. The spatial distribution of oocysts seeded into soil was examined by using conventional epifluorescence and DIC imaging (Fig. 2A, B) as well as confocal epifluorescence optical sectioning with stereo imaging (Fig. 2C). We found that for this work, the 63× (NA, 1.4) oil immersion DIC objective was optimum for this purpose. This lens provided the necessary bright fluorescence image intensity over a relatively broad field of vision with high *x*, *y*, and *z* resolution. Combined with an

electronic zoom factor of 30×, a final video screen image magnification that allowed for good resolution of both oocysts and bacterial cells in the surrounding soil matrix could be achieved (Fig. 2C). Use of the slow-scan setting for the laser (8 s per frame) and 16-line averaging during capture of each optical section greatly reduced background noise and improved image quality at the cost of increased capture time (approximately 2 min per section). A neutral-density filter (10% transmission) was placed in the laser path to reduce the laser intensity and thus reduce fading of the fluorescence during the extended period (approximately 32 min) of optical sectioning. When conventional DIC and epifluorescence images (Fig. 2A and B, respectively) were compared with the stereo images (Fig. 2C) of the same field, it was clear from the stereo images (Fig. 2C) that the oocysts seeded into the Collamer silt loam soil were not closely associated with AO-stained inorganic or organic soil particles containing soil bacteria. Stereo images showed oocysts that appeared to be suspended between soil particles rather than attached to them (Fig. 2C). In contrast to the confocal stereo image (Fig. 2C), the degree of association of oocysts with particles was difficult to assess in the conventional epifluorescence and DIC images (Fig. 2A and B).

Similar results were obtained with soil samples seeded up to 1 week prior to preparation for optical sectioning. These included the Trumansburg silt-clay fraction alone or mixed with the Collamer silt loam and seeded either with purified oocysts or with calf feces containing oocysts. The fact that oocysts were not found to closely associate with either soil, organic particles, or mineral particles in these soils may be explained by the use of the 0.1% NaPP dispersal reagent. However, we also examined oocysts in seeded soils and feces which were first suspended in distilled water or PBS and not dispersed with NaPP, with similar results. Also, empty and degraded oocyst fragments observed in the barnyard soil (Table 1) frequently appeared to be embedded in the soil matrix. These microscopic results suggest that fresh intact oocysts may have different surface properties than degraded oocysts. Indeed, preliminary electrophoretic mobility data suggest that fresh intact oocysts such as that shown in Fig. 2 may carry a neutral surface charge at circumneutral pH values (4a). Unlike the oocysts studied by Drozd and Schwartzbrod (15), which were reported to be negatively charged at neutral pH, our oocysts were purified by sucrose floatation and stored in distilled water. Apparently, oocyst surface hydrophobicity also may vary depending on the ionic strength of the suspending medium (15). Further research on the surface properties of oocysts purified under various conditions is needed before conclusions on this important topic can be reached.

Application of the dye permeability assay for testing viability of oocysts in soil. Routine microscopic analysis of samples with the dye permeability assay (9) was performed by using conventional epifluorescence and DIC microscopy imaged by the color CCD camera. The three fluorochromes employed in this assay (PI, FITC-conjugated antibody, and DAPI) could be visualized with the triple filter combination, but because of the weak DAPI fluorescence of the triple filter, we routinely used the UV filter combination (BP 360/40 excitation), which gave a much brighter blue fluorescence for DAPI. As noted by previous workers (8), the use of a CCD video camera boosted weak fluorescence signals by virtue of its longer scan times. In our system the optivar lens system was used to enlarge the image by 1.25 to 2 times, which facilitated the structural analysis of each oocyst. High-quality color images were captured for comparison with laser-scanned images on the LSM monitor or reproduction (see, e.g., Fig. 3 and 4) by using the color printer configured to receive RGB signals directly for the CCD video camera system. Another important advantage of using the color video camera system was reduction of user fatigue during long periods of sample observation by viewing fields on the CCD video monitor rather than through the microscope eyepieces. Ergonomic arrangement of the keyboard controls facilitated the *x*, *y*, and *z* movement of the stage and allowed comfortable viewing of the two video screens.

Three major dye permeability categories described by Campbell et al. (9) are shown in Fig. 3. In each column (A, B, and C) a *C. parvum* oocyst is seen by its DIC image (Fig. 3, row 1), by its epifluorescence image under the triple filter combination to reveal red PI and green FITC fluorescence (Fig. 3, row 2), and under UV excitation for DAPI (Fig. 3, row 3). The oocyst in Fig. 3, column A, was permeable to both PI (Fig. 3, column A, row 2) and DAPI (Fig. 3 column A, row 3). By the criteria established for this assay by Campbell et al. (9), the oocyst in column A should be considered nonviable (dead) by virtue of its permeability to PI and diffuse DAPI staining and by its lack of any distinct sporozoite structures and generally disorganized appearance in the DIC image (Fig. 3, column A, row 1). Note that PI (Fig. 3, column A, row 2) and DAPI (Fig. 3, column A, row 3) stained the entire oocyst, not just the nuclei. This diffuse staining pattern with both fluorochromes supports the interpretation of internal disorganization on the basis that intact (viable) sporozoites exclude PI but take up DAPI, which stains their nuclei (8, 9). A PI- and DAPI-permeable oocyst such as this would not be viable or infective. Note also that this oocyst also showed uneven (patchy) green FITC fluorescence on its outer surface (Fig. 3, column A, row 2). Such uneven immunofluorescence staining suggests that the outer surface layer of the wall carrying the antibody-recognized epitope may have been partly removed. This patchy fluorescence occurred randomly in unfixed oocyst samples (Fig. 3, row 2); however, it was more frequently seen on oocysts which are DAPI and PI permeable. Occasionally, in aged oocyst preparations, we observed a few oocysts that showed cytoplasmic DAPI fluorescence, such as that shown in Fig. 3, column A, row 3, but with no PI fluorescence (not illustrated). The DIC images of these oocysts also showed structural disorganization, as in Fig. 3, column A, row 1. Such diffuse DAPI staining of disorganized internal sporozoite structures suggested that degradation of the nuclear membrane and other internal membranes had occurred, but PI did not pass through the oocyst wall. Clearly the disorganization of sporozoite membranes, especially in aged oocyst preparations, would be a sign of cellular death and would agree with the interpretation of this staining pattern by Campbell et al. (10). PI-negative, DAPI-negative oocysts are also considered to be viable, but with the caveat that some treatment, e.g., acidification, is required before excystation will occur (9). For the purposes of this paper, we considered viable oocysts to include the "potentially infectious" oocysts (i.e., DAPI-positive and -negative, PI-negative oocysts); however, Robertson et al. (36), described viable oocysts to be those which could excyst in a 4-h excystation protocol without a further trigger (i.e., the DAPI-positive, PI-negative oocysts).

Oocysts satisfying the criteria of Campbell et al. (9) for the potentially infectious categories are shown in Fig. 3, columns B and C. These oocysts all showed intact sporozoite structures with DIC (Fig. 3, columns B and C, row 1); however, in some focal planes, the sporozoite structures could not be seen, except when focused at a lower plane (not illustrated) (e.g., upper oocyst in Fig. 3, column B, row 1). In the lower oocyst in Fig. 3, column B, row 1, three distinct sporozoites are easily recognized. The triple filter epifluorescence image of this oo-

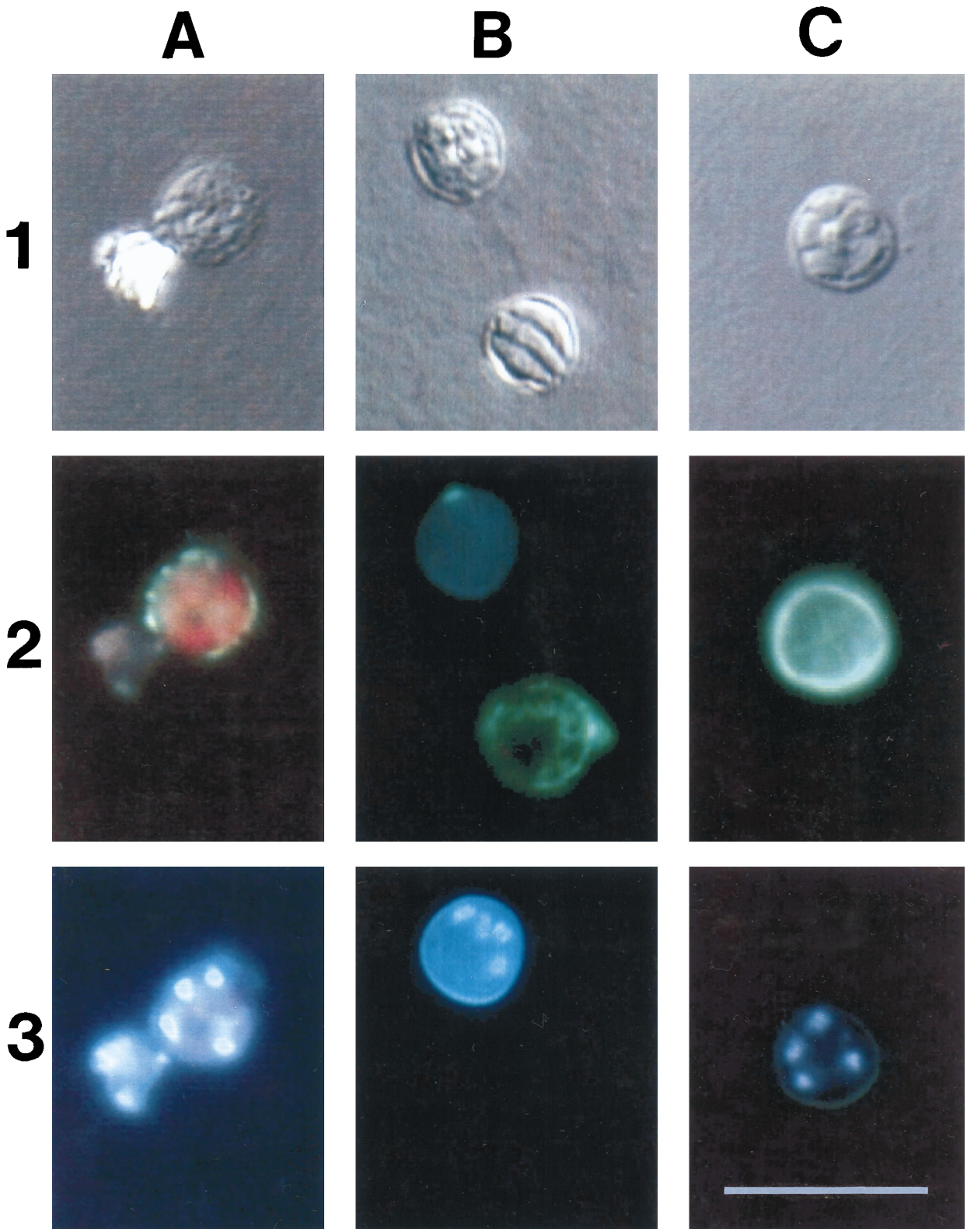

FIG. 3. Matrix of color CCD video images illustrating the results of the dye permeability assay including IF staining as applied to *C. parvum* oocysts suspended in distilled water (columns A and B) and in a fecal slurry (column C) (see Materials and Methods). Each column shows the same field of view recorded under three different imaging conditions (row 1, DIC; row 2, PI and FITC epifluorescence; row 3, DAPI epifluorescence). See text for details and interpretation of the images. The primary color images used to create this figure were captured by the color CCD camera with conventional DIC and epifluorescence and the Zeiss 100× (NA, 1.3) oil immersion DIC lens combined with the 2× optivar. Bar, 10 μm.

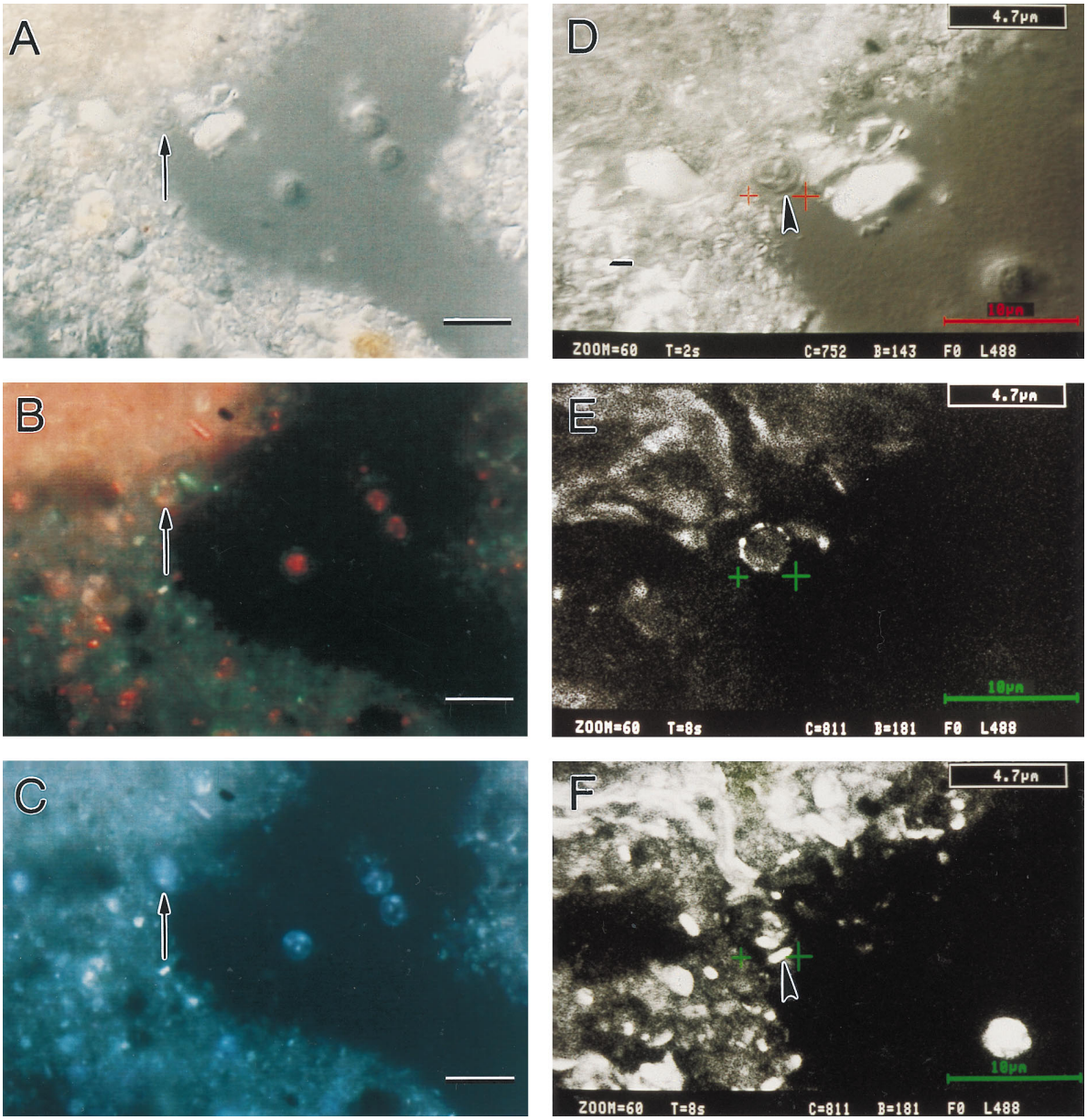

FIG. 4. Comparison of color CCD video (A, B, and C) and confocal laser-scanned (D, E, and F) images of the same microscopic field showing heat-treated *C. parvum* oocysts seeded into the Collamer silt loam soil. Before seeding, the oocyst suspension was placed in a boiling water bath for 5 min to convert all oocysts to dye-permeable (dead) oocysts (for example, see Fig. 3, column A). The soil was then seeded with 10^6 heat-treated oocysts per g. The dye permeability assay procedure with IF staining was applied in suspension as described in Materials and Methods. Three of the four oocysts present in the field can be clearly seen in the right-center of the conventional DIC (A), PI-FITC epifluorescence (B), and DAPI epifluorescence (C) images. The fourth oocyst is obscured by soil particles (arrows in panels A, B, and C). The obscured oocyst is more clearly discerned at a slightly higher magnification in the laser-scanned DIC image (D). Sporozoites (arrowhead in panel D) and an adjacent residual body (above the sporozoites) are now visible inside the oocyst. The confocal epifluorescence image made with the green emission signal (E) shows the FITC-IF fluorescence signal outlining the oocyst wall. Two PI-stained sporozoites are also seen in the confocal epifluorescence red emission image (arrowhead in panel F). Note that the green FITC-IF-fluorescence (barely visible; arrow in panel B) is clearly revealed in the green emission confocal epifluorescence image (E). Similarly, the sporozoites seen in the DIC image (arrow in panel A) are more clearly seen in the laser-scanned DIC image (arrowhead in panel D) and the confocal red epifluorescence image (arrowhead in panel F). All images were made through the 100× (NA, 1.3) oil immersion Neofluar DIC lens. The images in panels A to C were captured with the color CCD camera and recorded with the color printer. The laser-scanned images (D to F) were recorded by using LSM 210 software with the 488-nm laser line, 16-line averaging, and a zoom factor of 60× (final magnification, ×6,000). Bars, 10 µm.

cyst (Fig. 3, column B, row 2) shows only the patchy green FITC fluorescence of the IF stain and no red PI fluorescence, clearly indicating that PI was excluded from these oocysts (compare Fig. 3, columns A and B, row 2). In Fig. 3, column B, row 3, note that four sporozoite nuclei were highlighted by DAPI fluorescence in the upper oocyst, but no DAPI fluorescence is seen in the lower oocyst. The upper oocyst in Fig. 3, column B, row 3, and the one in Fig. 3, column C, row 3, would be considered viable by the criteria of Campbell et al. (9), being PI negative and showing only nuclear DAPI staining, with recognizable internal sporozoite structure as seen in the DIC images (Fig. 3, columns B and C, row 1). It is worth noting that the diffuse DAPI fluorescence seen in the nonnuclear regions of the upper oocyst in Fig. 3, column B, row 3, suggests

that this oocyst was more permeable to DAPI than the one in Fig. 3, column C, row 3, and therefore, as pointed out by Robertson et al. (36, 38) and Campbell et al. (10) could be more vulnerable to antagonistic environmental factors. However, since the curved sporozoite bodies are not highlighted by DAPI, this oocyst is still considered viable. The lower oocyst in Fig. 3, column B, row 3, did not take up DAPI at all. Indeed, it seemed to disappear under UV excitation. Thus, according to Campbell et al. (9), this oocyst, being PI negative (Fig. 3, column B, row 2), DAPI negative (Fig. 3, column B, row 3), and with good DIC structure (Fig. 3, column B, row 1), would represent the most impermeable and, therefore, environmentally resistant form of oocyst. This category of oocyst was found to be the most abundant category in fresh calf feces (21, 36) and human stools from individuals with cryptosporidiosis. It is also the most refractile under DIC and has the most distinct internal sporozoite structure. In complex matrices such as feces or soil where high levels of DAPI background staining can occur, these oocysts appeared under UV excitation as "black holes" in a cloud of bluish-white DAPI fluorescence. It is important to note that empty oocysts (ghosts) (not illustrated) were also recognized by green FITC fluorescence. These dead oocysts also were PI negative and DAPI negative, but they never showed the black hole phenomenon, and their DIC images revealed no internal sporozoite structure.

In viable oocysts with the most typical DAPI staining pattern (Fig. 3, column C), distinct sporozoites were seen in DIC imaging (Fig. 3, column C, row 1); under the triple filter (Fig. 3, column C, row 2), PI was excluded, and under UV excitation (Fig. 3, column C, row 3), four distinct DAPI-positive nuclei were seen without any diffuse staining of other sporozoite structures. Note that in Fig. 3, column C, row 2, lines of slightly brighter green FITC fluorescence in an X shape were seen in the center of this oocyst. We considered such lines to represent characteristic folds in the oocyst envelope, as reported by Robertson et al. (37).

Several other nonviable staining patterns were often observed (not illustrated) in old or degraded samples. They usually showed little or no PI fluorescence and diffuse, dim DAPI fluorescence arising from residual bodies or other unidentifiable material in partly empty oocysts. Occasionally, we observed oocysts containing one, two, or three sporozoites of the four or a residual body that showed bright but diffuse DAPI staining of internal contents (as in Fig. 3, column A, row 3), with the remaining sporozoite(s) showing a well-defined DAPI-positive nucleus (as in Fig. 3, column B, row 3). For safety in using this assay for viability assessment of environmental samples, we would have to consider such oocysts to be viable. We reason that even though their ability to survive under natural conditions, such as would exist in natural waters, soils, or sediments, may be remote (34), the survivability of some oocysts may be altered and enhanced by exposure to chemical, physical, or biological factors in bovine feces (2, 36).

Once the dye permeability assay was standardized as described above, we proceeded to modify the protocol for application directly to unwashed fecal samples and to seeded or naturally contaminated soil and barnyard sediment. The modifications in soils and sediments involved dispersal of particulate material with NaPP and, for all samples, mounting the final suspension on an agar-coated slide. Otherwise, the staining procedures were unaltered from those used for Fig. 3. In aged seeded soil samples where the oocysts may have partially degraded, it was often difficult to find and positively identify oocysts embedded in matrix material with high background fluorescence (Fig. 4A, B, and C). An additional problem was that the FITC signal was often weak or the immunostaining was patchy (e.g., Fig. 3, columns A and B, row 2). In these instances, scanning confocal images of separate green FITC and red PI epifluorescence emission signals as shown in Fig. 4D, E, and F (see legend for details) allowed for identification of oocysts and determination of their viability without interference from the out-of-focus background fluorescence. For such samples, the concomitant use of the color video imaging with confocal laser scanning black-and-white imaging as described above and the availability of LSM electronic zoom factors and measurement programs allowed accurate analysis of oocyst structure even when the oocysts were buried in the soil matrix (Fig. 4). The use of the multiple imaging options of the LSM system along with its computer-assisted features, such as slow scanning times and 16-line averaging, further improved image quality. These advantages greatly increase operator confidence for identification of oocysts in the soil matrix.

ACKNOWLEDGMENTS

This work was supported in part by funds from the USDA Competitive Research Grant Program, the U.S. Department of Interior through the NYS Water Resources Institute at Cornell, the Center for Advanced Technology (CAT) at Cornell in Biotechnology sponsored by the New York State Science and Technology Foundation (a consortium of industries and the National Science Foundation), the NYC Watershed Whole Farm Program through the New York State Water Resources Institute, and the College of Agriculture and Life Sciences at Cornell. The LSM was purchased under a grant from the USDOE Instrumentation Program (no. DE-FG05-90ER75580).

We are grateful to D. Bowman and M. Frongillo for providing purified oocysts, to M. Walker and C. Brush for kindly providing unpublished observations, and to Rhea E. Garen for photographic assistance and art work in preparing the figures. We extend special thanks to M. Jenkins for his helpful editorial comments and to W. Jakubowski, who also provided helpful critical comments and additional references to the manuscript. The expert secretarial assistance of Patti Lisk is gratefully acknowledged.

REFERENCES

1. **American Society for Testing and Materials.** 1992. Proposed test method for *Giardia* cysts and *Cryptosporidium* oocysts in low-turbidity water by a fluorescent antibody procedure. Proposal P229, p. 925–935. *In* 1992 annual book of ASTM standards, section 11. American Society for Testing and Materials, Philadelphia, Pa.
2. **Anguish, L. J., M. J. Walker, D. D. Bowman, W. C. Ghiorse, and M. B. Jenkins.** Dye permeability and determination of survival kinetics of *Cryptosporidium parvum* oocysts. Submitted for publication.
3. **Beloin, R. M., J. L. Sinclair, and W. C. Ghiorse.** 1988. Distribution and activity of microorganisms in subsurface sediments of a pristine study site in Oklahoma. Microb. Ecol. **16:**85–97.
4. **Bloem, J., M. Veninga, and J. Shepherd.** 1995. Fully automatic determination of soil bacterium numbers, cell volumes, and frequencies of dividing cells by confocal laser scanning microscopy and image analysis. Appl. Environ. Microbiol. **61:**926–936.

4a. **Brush, C. (Cornell University).** Personal communication.

5. **Caldwell, D. E.** 1993. The potential of scanning confocal laser microscopy in studies of groundwater communities, E-01. *In* Abstracts of the Second International Symposium on Subsurface Microbiology, Bath, England.
6. **Caldwell, D. E., D. R. Korber, and J. R. Lawrence.** 1992. Imaging of bacterial cells by fluorescence exclusion using scanning confocal laser microscopy. J. Microbiol. Methods **15:**249–261.
7. **Caldwell, D. E., D. R. Korber, and J. R. Lawrence.** 1992. Confocal laser microscopy and digital image analysis in microbial ecology. Adv. Microb. Ecol. **12:**1–67.
8. **Campbell, A. T., R. Haggart, L. J. Robertson, and H. V. Smith.** 1992. Fluorescent imaging of *Cryptosporidium* using a cooled charge couple device (CCD). J. Microbiol. Methods **16:**169–174.
9. **Campbell, A. T., L. J. Robertson, and H. V. Smith.** 1992. Viability of *Cryptosporidium parvum* oocysts: correlation of in vitro excystation with inclusion or exclusion of fluorogenic dyes. Appl. Environ. Microbiol. **58:**3488–3493.
10. **Campbell, A. T., L. J. Robertson, and H. V. Smith.** 1993. Effects of preservatives on viability of *Cryptosporidium parvum* oocysts. Appl. Environ. Microbiol. **59:**4361–4362.
11. **Chapman, P. A., and B. A. Rush.** 1990. Efficiency of sand filters for removing *Cryptosporidium* oocysts from water. J. Med. Microbiol. **32:**243–245.

12. **Czymmek, K. J., J. H. Whallon, and K. L. Klomparens.** 1994. Confocal microscopy in mycological research. Exp. Mycol. **18:**275–293.
13. **D'Antonio, R. G., R. E. Winn, and R. Jajae.** 1985. Sequential acute gastroenteritis from contaminated drinking water caused by Norwalk virus and *Cryptosporidium*. Clin. Res. **33:**399.
14. **Distel, D. L., and C. M. Cavanaugh.** 1994. Independent phylogenetic origins of methanotrophic and chemoautotrophic bacterial endosymbioses in marine bivalves. J. Bacteriol. **176:**1932–1938.
15. **Drozd, C., and J. Schwartzbrod.** 1996. Hydrophobic and electrostatic cell surface properties of *Cryptosporidium parvum*. Appl. Environ. Microbiol. **62:**1227–1232.
16. **Fayer, R.** 1994. Effect of high temperature on infectivity of *Cryptosporidium parvum* oocysts in water. Appl. Environ. Microbiol. **60:**2732–2735.
17. **Fayer, R., and T. Nerad.** 1995. Effects of low temperatures on viability of *Cryptosporidium parvum* oocysts. Appl. Environ. Microbiol. **62:**1431–1433.
18. **Ghiorse, W. C.** 1993. Use of the confocal laser scanning microscope for detecting viable, but unculturable subsurface bacteria, B-33. *In* Abstracts of the Second International Symposium on Subsurface Microbiology, Bath, England.
19. **Ghiorse, W. C., D. N. Miller, R. L. Sandoli, and P. L. Siering.** 1995. Applications of laser scanning microscopy for analysis of aquatic microhabitats. Microsc. Res. Tech. **33:**73–86.
20. **Grimason, A. M., H. V. Smith, J. F. W. Parker, Z. Bukhari, A. T. Campbell, and L. J. Robertson.** 1994. Application of DAPI and immunofluorescence for enhanced identification of *Cryptosporidium* spp. oocysts in water samples. Water Res. **28:**733–736.
21. **Haldeman, D. L., P. S. Amy, D. Ringelberg, D. C. White, R. E. Garen, and W. C. Ghiorse.** 1995. Microbial growth and resuscitation alter community structure after perturbation. FEMS Microbiol. Ecol. **17:**27–38.
22. **Hayes, E. B., T. D. Matte, T. R. O'Brian, T. W. McKinley, G. S. Logsdon, J. B. Rose, B. L. P. Ungar, D. M. Word, P. F. Pinsky, M. L. Cummings, M. A. Wilson, E. G. Long, E. S. Hurwitz, and D. D. Juranek.** 1989. Contamination of a conventionally treated filtered public water supply by *Cryptosporidium* associated with a large community outbreak of cryptosporidiosis. N. Engl. J. Med. **320:**1372–1376.
23. **Jakubowski, W., S. Boutros, W. Faber, W. Ghiorse, M. LeChevallier, J. Rose, S. Schaub, A. Singh, and M. Stewart.** 1996. Status of environmental methods for Cryptosporidium. A report prepared by Technical Task Force E, CDC Working Group on Waterborne *Cryptosporidiosis*. J. Am. Water Works Assoc. **88:**107–121.
24. **Korber, D. R., G. A. James, and J. W. Costerton.** 1994. Evaluation of fleroxacin activity against established *Pseudomonas fluorescens* biofilms. Appl. Environ. Microbiol. **60:**1663–1669.
25. **Korber, D. R., J. R. Lawrence, M. J. Hendry, and D. E. Caldwell.** 1993. Analysis of spatial variability within MOT^+ and MOT^- *Pseudomonas fluorescens* biofilms using representative elements. Biofouling **7:**339–358.
26. **Laurent, M., G. Johannin, N. Gilbert, L. Lucas, D. Cassio, P. X. Petit, and A. Fleury.** 1994. Power and limits of laser scanning confocal microscopy. Biol. Cell **80:**229–240.
27. **Lawrence, J. R., D. R. Korber, B. D. Hoyle, J. W. Costerton, and D. E. Caldwell.** 1991. Optical sectioning of microbial biofilms. J. Bacteriol. **173:** 6558–6567.
28. **Lens, P., A. Massone, A. Rozzi, and W. Verstraete.** 1994. The effect of sulfate reducing bacteria on the treatment performance of aerobic biofilm reactors, p. 58–60. *In* Second International Symposium on Environmental Biotechnology. Chameleon Press Ltd., London, England.
29. **MacKenzie, W. R., N. J. Hoxie, M. E. Proctor, M. S. Gradus, K. A. Blair, D. E. Peterson, J. J. Kazmierczak, D. G. Addiss, K. R. Fox, J. B. Rose, and J. P. Davis.** 1994. Massive waterborne outbreak of *Cryptosporidium* infection associated with a filtered water supply. N. Engl. J. Med. **331:**161–167.
30. **Madore, M. S., J. B. Rose, C. P. Gerba, M. J. Arrowood, and C. R. Sterling.** 1987. Occurrence of *Cryptosporidium* oocysts in sewage effluents and select surface waters. J. Parasitol. **73:**702–705.
31. **Madsen, E. L.** 1996. A critical analysis of methods for determining the composition and biogeochemical activities of soil microbial communities in situ, p. 287–370. *In* G. Stotzky, and J.-M. Bollag (ed.), Soil biochemistry, vol. 9. Marcel Dekker, New York, N.Y.
32. **Massol-Deya, A. A., J. Whallon, R. F. Hickey, and J. M. Tiedje.** 1995. Channel structures in aerobic biofilms of fixed-film reactors treating contaminated groundwater. Appl. Environ. Microbiol. **61:**769–777.
33. **Moore, A. C., B. L. Herwaldt, G. F. Craun, R. L. Calderon, A. K. Highsmith, and D. D. Juranek.** 1994. Waterborne disease in the United States, 1991 and 1992. J. Am. Water Works Assoc. **86:**87–99.
34. **Ongerth, J. E., and H. H. Stibbs.** 1987. Identification of *Cryptosporidium* oocysts in river water. Appl. Environ. Microbiol. **53:**672–676.
35. **Parker, J. F. W., and H. V. Smith.** 1993. Destruction of oocysts of *Cryptosporidium parvum* by sand and chlorine. Water Res. **27:**729–731.
36. **Robertson, L. J., A. T. Campbell, and H. V. Smith.** 1992. Survival of *Cryptosporidium parvum* oocysts under various environmental pressures. Appl. Environ. Microbiol. **58:**3494–3500.
37. **Robertson, L. J., A. T. Campbell, and H. V. Smith.** 1993. Induction of folds or sutures on the walls of *Cryptosporidium parvum* oocysts and their importance as a diagnostic feature. Appl. Environ. Microbiol. **59:**2638–2641.
38. **Robertson, L. J., A. T. Campbell, and H. V. Smith.** 1993. In vitro excystation of *Cryptosporidium parvum*. Parasitology **106:**13–19.
39. **Rodgers, M. R., D. F. Flanigan, and W. Jakubowski.** 1995. Identification of algae which interfere with the detection of *Giardia* cysts and *Cryptosporidium* oocysts and a method for alleviating this interference. Appl. Environ. Microbiol. **61:**3759–3763.
40. **Rose, J. B.** 1988. Occurrence and significance of *Cryptosporidium* in water. J. Am. Water Works Assoc. **80:**53–58.
41. **Rose, J. B.** 1990. Occurrence and control of *Cryptosporidium* in drinking water, p. 294–321. *In* G. A. McFeters (ed.), Drinking water microbiology, progress and recent developments. Springer-Verlag, New York, N.Y.
42. **Rose, J. B., H. Darbin, and C. P. Gerba.** 1988. Correlations of the protozoa, Cryptosporidium and *Giardia* with water quality variables in a watershed, p. 43-1–43-6. *In* Proceedings, International Conference on Water and Wastewater Microbiology, vol. 2.
43. **Rose, J. B., L. K. Landeen, K. R. Riley, and C. P. Gerba.** 1989. Evaluation of immunofluorescence techniques for detection of *Cryptosporidium* oocysts and *Giardia* cysts from environmental samples. Appl. Environ. Microbiol. **55:**3189–3196.
44. **Trolldenier, G.** 1973. The use of fluorescence microscopy for counting soil microorganisms, p. 53–59. *In* T. Rosswall (ed.), Modern methods in the study of microbial ecology. Bulletins from the Ecological Research Committee, Swedish Natural Sciences Research Council, vol. 17. Swedish Natural Sciences Research Council, Stockholm, Sweden.
45. **Vesey, G., J. S. Slade, M. Byrne, K. Shepherd, P. J. Dennis, and C. R. Fricker.** 1993. Routine monitoring of *Cryptosporidium* oocysts in water using flow cytometry. J. Appl. Bacteriol. **75:**87–90.
46. **Vesey, G., N. Ashbolt, G. Wallner, M. Dorsch, K. Williams, and D. Veal.** 1995. Assessing *Cryptosporidium parvum* oocyst viability with fluorescent *in situ* hybridisation using ribosomal RNA probes and flow cytometry, p. 133–138. *In* W. C. Betts, D. Casemore, C. Fricker, H. Smith, and J. Watkins (ed.), Protozoan parasites and water. The Royal Society of Chemistry, London, England.

46a. **Walker, M. (Cornell University).** Unpublished observations.

47. **Wolfaardt, G. M., J. R. Lawrence, J. V. Headley, R. D. Robarts, and D. E. Caldwell.** 1994. Microbial exopolymers provide a mechanism for bioaccumulation of contaminants. Microb. Ecol. **27:**279–291.
48. **Wolfaardt, G. M., J. R. Lawrence, R. D. Robarts, S. J. Caldwell, and D. E. Caldwell.** 1994. Multicellular organization in a degradative biofilm community. Appl. Environ. Microbiol. **60:**434–446.